ELSEVIER

Journal of Hazardous Materials 60 (1998) 1–28

JOURNAL OF HAZARDOUS MATERIALS

Containment mechanism of trivalent chromium in tricalcium silicate

O.E. Omotoso [a], D.G. Ivey [b,*], R. Mikula [a]

[a] *CANMET Western Research Centre, Devon, Alberta TOC 1E0, Canada*
[b] *Department of Chemical and Materials Engineering, University of Alberta, Edmonton, Alberta T6G 2G6, Canada*

Received 15 October 1996; accepted 15 February 1997

Abstract

Trivalent chromium admixtures in ordinary Portland cement (OPC) have a pronounced effect on the structure of the hydration products of tricalcium silicate (C_3S). [1] Cr^{III} compounds, added as dopants to C_3S, simulate chromium waste forms that might be stabilized in a Portland cement matrix. Scanning electron microscopy (SEM) and transmission electron microscopy (TEM), were used to identify the microstructural changes accompanying the addition of Cr^{III} solutions to C_3S. Energy dispersive spectroscopy (EDS) was used to probe the distribution of chromium in the stabilized hazardous waste forms. Fourier transform infrared (FTIR) and ^{29}Si nuclear magnetic resonance (NMR) spectroscopies were employed to provide structural information about the crystalline and amorphous products of C_3S hydration. In monolithic waste forms containing trivalent chromium, chromium was found to be stabilized both through the formation of insoluble calcium chromium hydroxide nitrate complexes, and localized chemical incorporation of chromium in the stable calcium silicate hydrate (C-S-H) phase. © 1998 Elsevier Science B.V.

Keywords: Stabilization; Chromium; Tricalcium silicate; Ordinary Portland cement; Electron microscopy; Fourier transform infrared spectroscopy; Nuclear magnetic resonance spectroscopy

1. Introduction

A fully hydrated C_3S [1] paste contains amorphous calcium silicate hydrate (C-S-H), calcium hydroxide (CH) and calcium carbonate introduced into the matrix from partial

* Corresponding author. Fax: +1 403 492 2881.

[1] Cement notations. C:CaO; S:SiO_2; A:Al_2O_3; F:Fe_2O_3; H:H_2O; CH:$Ca(OH)_2$; C_3S:Ca_3SiO_5; C-S-H:Calcium silicate hydrate; Aft:Alumino-ferrite-tri; Afm:Alumino-ferrite-mono.

PII S0304-3894(97)00037-X

carbonation of CH and C-S-H. The microstructural and chemical development of these hydration products of C_3S have been extensively studied using electron microscopy and X-ray microanalysis. These techniques have also been used to probe the distribution of hazardous heavy metal ions in solidified and stabilized waste forms. Scanning electron microscopy (SEM) is primarily used for analyzing fractured and polished surfaces [1–5]. The high spatial resolution of transmission electron microscopy (TEM) coupled with X-ray microanalysis on a nanoscale make TEM a better tool than SEM for probing the location of metal ions in solidified waste forms.

Because of the amorphous nature of C-S-H, the most important product of C_3S hydration, diffraction techniques have found limited application in structural characterization of C-S-H and other amorphous phases that may contain heavy metal ions. Fourier transform infrared (FTIR) and nuclear magnetic resonance (NMR) spectroscopies have been helpful in gaining an insight into the structure of these amorphous phases. SEM/TEM and X-ray microanalysis studies by Heimann et al. [6] and Ivey et al. [7] indicated that Cr^{III} dissolves in all the hydration products of ordinary Portland cement (OPC). When added in high concentrations (~ 1.0 M Cr^{III}), highly leach-resistant chromium-rich regions are identifiable. In addition, Cr^{3+} appears to substitute for Si^{4+} in C-S-H. FTIR and SEM studies by Mollah et al. [8] lend credence to Cr^{3+} substitution for Si^{4+}, with K^+ acting to compensate for charge deficiencies. An earlier similar observation was made by Tashiro et al. [9], differing only in the latter's inference that Cr^{3+} substitutes for both Ca^{2+} and Si^{4+}. Butler et al. [10] studied the OPC/Cr^{III} system using ^{29}Si NMR. It was reported that Cr^{III} retarded polymerization of the orthosilicate units (Q_o), since no dimeric (Q_1) or polymeric (Q_2) silicate units were observed in the spectra. In an extensive TEM and X-ray diffraction (XRD) investigation by Kindness et al. [11], C_3S, CH, C_3A and C-S-H were doped with 0.0019 M and 0.0048 M Cr^{3+} at a w:s ratio of ~ 100. The CH/Cr^{3+} system hydrated at 55°C appeared to form $Ca_2Cr(OH)_7 \cdot 3H_2O$, an isomorph of $Ca_2Al(OH)_7 \cdot 3H_2O$. At 25°C, an isomorph of $Ca_2Al_2O_5 \cdot 3H_2O$ was observed (Ca/Cr = 0.28). Similar products were observed in the C_3A/Cr^{3+} system. Based on these observations, it was concluded that Cr^{3+} could substitute for Al in most of the calcium aluminate hydrate phases present in OPC. In C_3S/Cr^{3+} experiments, however, a crystalline phase (Ca:Cr ~ 0.74) with $\sim 2\%$ Si was observed. The Si was attributed to contribution from neighbouring C-S-H (X-ray microanalysis in the TEM). XRD indicated that $Cr(OH)_3 \cdot 3H_2O$ had formed. $Cr(OH)_3 \cdot 3H_2O$ was also observed to form in C-S-H/Cr^{3+} systems. No evidence of Cr incorporation in C-S-H was found. It is somewhat difficult to relate these findings to previous ones because of the high w:s ratio employed in synthesizing the hydrated phases.

Richardson and Groves [12] modeled the incorporation of trivalent metal ions R^{3+} (Al^{3+} and Fe^{3+}) in C-S-H. It was found from TEM microanalysis that a linear relationship exists between the R:Ca atom ratio and the Si:Ca ratio as shown in Eq. (1):

$$\text{Si:Ca} = 0.444 + 2.25(\text{R:Ca}) \quad (1)$$

This is in contrast to the results obtained with X-ray microanalysis in the SEM, whereby R:Ca increases with decreasing Si:Ca ratio [13,14]. Richardson and Groves [12] proposed the formation of a series of C-S-H phases with a range of Ca:Si ratios in which

the same fraction of Si atoms are replaced by Al or Fe in each phase. R:Ca will thus increase as the Ca:Si ratio decreases.

This study attempts to understand the mechanism of chromium containment in C_3S. To achieve this objective, various analytical tools were used to probe the structural, morphological and chemical characteristics of the phases formed during the hydration of Cr^{III}-doped C_3S.

2. Materials and methods

The preparation of C_3S has been described elsewhere [15]. Reagent grade $Cr(NO_3)_3 \cdot 9H_2O$ solutions containing 0.1 M, 1 M, 2 M and 2.75 M concentrations were mixed with C_3S in a solution:C_3S ratio of ~ 0.5. The 0.1-M and 1-M pastes were hydrated for 1 and 60 days while the 2-M pastes were hydrated for 5 min, 6 h, 1 day, 3 days and 60 days. The 2.75-M pastes were hydrated for 14 months. Except for one set of the 14-month-old 2.75 M Cr^{III} paste, which was cast and sealed inside a polyethylene bottle, all the other samples were cast into plastic moulds and placed (uncovered) in a humidifying chamber flushed with N_2.

The concentration of typical chromium waste streams is ~ 0.1 M. However, 1 M, 2 M and 2.75 M Cr^{III} solutions were employed in these experiments to increase the chances of positively identifying chromium containing phases. Blank pastes were prepared for each hydration period by mixing C_3S with distilled water (w:s = 0.5).

2.1. Scanning electron microscopy

A Hitachi S-2700 scanning electron microscope equipped with a Link eXL energy dispersive spectrometer (EDS) was used for microstructural and microanalytical characterization of the hydrated samples. Both fractured and epoxy-impregnated polished samples were used. An accelerating voltage of 20 kV was used for imaging and microanalysis. X-ray data was acquired for 100 s live time at > 2500 cps. Unreacted C_3S in the hydrating pastes and $CaCrO_4 \cdot 2H_2O$ were used as standards to calculate the Ca:Si and the Ca:Cr ratios in the hydrate phases.

2.2. Transmission electron microscopy

Characterization in the TEM was done on a JEOL 2010 transmission electron microscope equipped with a Noran Ge energy dispersive detector. The method described by Ivey et al. [7] was used for the preparation of thin sections. The probe size used for compositional analysis was ~ 10 nm and data was collected for 100 s live time. Quantification is simpler than in the SEM, since for a thin specimen, absorption and fluorescence effects are negligible. The weight ratio of two elements are then proportional to their X-ray intensities.

$$\frac{C_A}{C_B} = k_{A/B}\frac{I_A}{I_B} \tag{2}$$

C_A and C_B are the concentrations in wt.% of elements A and B, I_A and I_B are the respective X-ray intensities, and $k_{A/B}$ is the Cliff–Lorimer factor. The *k*-factors were determined by analyzing areas containing unhydrated C_3S and $CaCrO_4 \cdot 2H_2O$.

2.3. Fourier transform infrared spectroscopy

Powdered samples $< 5\ \mu$m in size were used for FTIR spectroscopy. The classical disk technique was used with caesium iodide pellets to prepare FTIR samples. The spectra were collected on a Nicolet 750 Magna spectrometer between 400 and 4000 cm^{-1}. Assignments of the vibrational frequencies in the hydrate complexes were aided by partial deuteration of the OH^- groups [16].

2.4. Nuclear magnetic resonance spectroscopy

Powdered samples were also used for ^{29}Si solid-state NMR. The high-resolution NMR spectra were recorded at 59.63 MHz on a Bruker M SL-300 spectrometer. Samples were spun at 4.5 kHz at the magic angle to the external field. A relaxation delay of 10 s was used for all samples. About 5000 scans were generally collected. This yielded satisfactory signal-to-noise ratio in most cases. Q_8M_8 (trimethylsilyl ester of the four ring octameric silicate) was used as the secondary standard. Its major ^{29}Si chemical shift was assigned as $+11.5$ ppm downfield from TMS (tetramethylsilane). Identification of the different silicate polyhedra was made based on the works of Lippmaa et al. [17,18].

Ratios of the Q_1 (dimeric silicate) to Q_2 (polymeric silicate) were obtained by fitting a Voigt function to the peaks and integrating.

3. Results and discussion

3.1. Microstructure and composition of Cr^{III}-doped pastes

Fig. 1a,b show typical SEM micrographs of C-S-H in 1-day-old blank and 0.1 M Cr^{III} nitrate pastes, respectively. In addition to the fibrous morphology of C-S-H in the blank paste, C-S-H structures resembling flowering buds are discernible in the 1-day-old 0.1 M Cr^{III} nitrate pastes. No chromium was found in this type of C-S-H. The formation of the ‘flowering bud-like C-S-H’ signifies the modifying effects low concentrations of chromium and nitrate ions have on the morphology of the hydration products. Chromium and nitrate ions are known to be good hydration accelerators [19,20]. As shown in Table 1, X-ray microanalysis in the TEM gave a more variable C-S-H concentration than X-ray microanalysis in the SEM. The average Ca:Si ratios of the C-S-H obtained from

Fig. 1. SEM micrographs of 1- and 60-day-old pastes: (a) 1-day-old blank paste showing fibrous C-S-H; (b) 1-day-old 0.1 M Cr^{III} paste showing a different morphology of C-S-H; (c) 60-day-old blank paste; and (d) 60-day-old 0.1 M Cr^{III} paste.

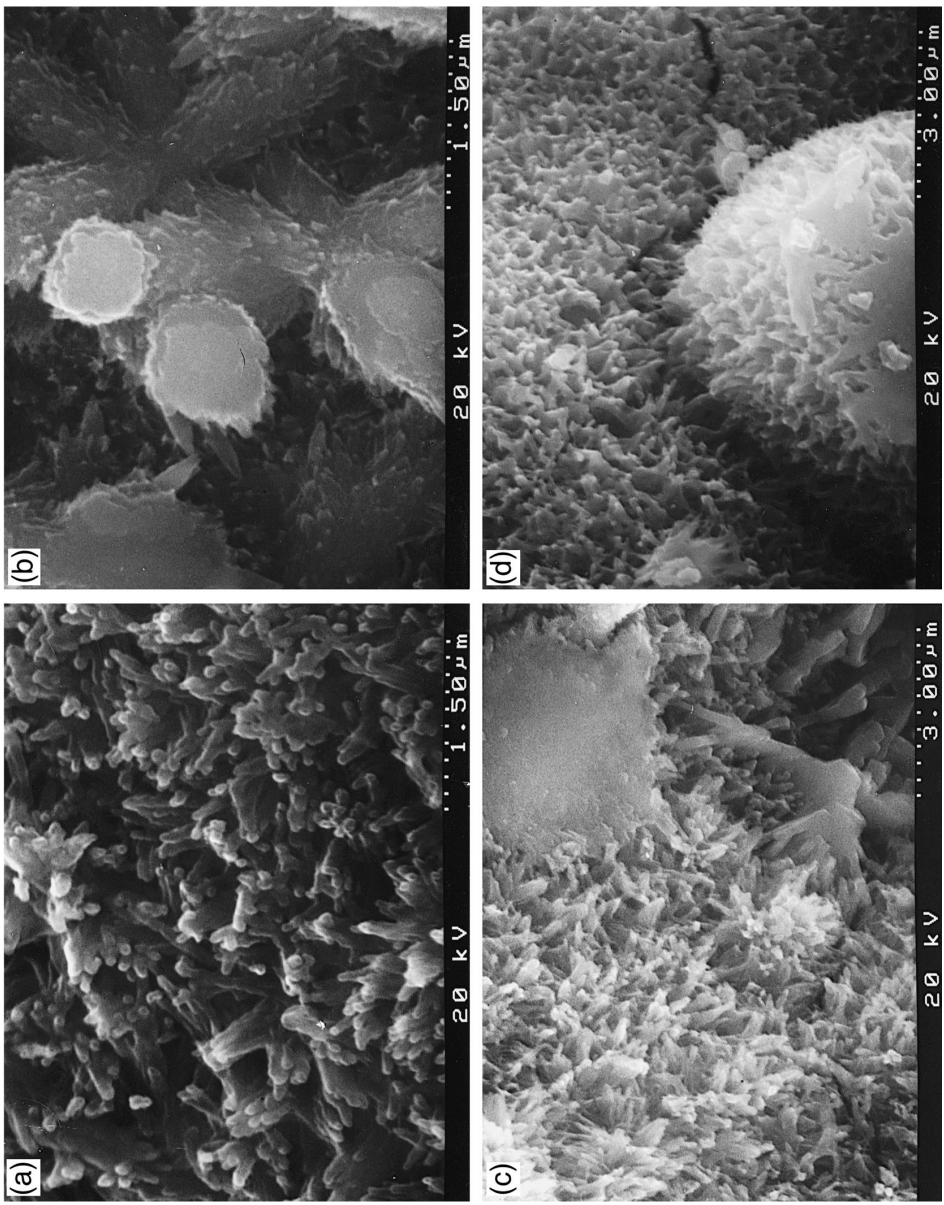
(a)
20 kV
1.50µm
(b)
20 kV
1.50µm
(c)
20 kV
3.00µm
(d)
20 kV
3.00µm

Table 1
Average Ca:Si ratios in hydrated blank and chromium-doped pastes

Sample	Ca:Si ratio (SEM $\pm \sigma$)	Ca:Si ratio (TEM $\pm \sigma$)
Blank: 1 day	1.65 ± 0.02	1.10 ± 0.35 (0.83 to 1.49)
Blank: 14 months	1.61 ± 0.15	1.24 ± 0.54 (0.52 to 2.04)
0.1 M Cr^{III}: 1 day	1.60 ± 0.05	1.15 ± 0.16 (0.95 to 1.30)
0.1 M Cr^{III}: 60 days	1.54 ± 0.05	n.d.
1 M Cr^{III}: 1 day	1.87 ± 0.07	n.d.
1 M Cr^{III}: 60 days	n.d.	1.5 ± 0.4 (0.8 to 2.0)
2 M Cr^{III}: 5 min	n.d.	1.7 ± 0.3 (1.12 to 2.06)
2 M Cr^{III}: 1 day	n.d.	1.04 ± 0.18 (0.83 to 1.48)
2 M Cr^{III}: 60 days	n.d.	(a) 0.48 ± 0.09 (0.39 to 0.62) (b) 1.59 ± 0.35 (0.88 to 2.18)
2.75 M Cr^{III}: 14 months	1.83 ± 0.15	n.d.

σ: standard deviation.
n.d.: not determined.

SEM/EDS are 1.65 ± 0.02 and 1.60 ± 0.05 for the blank and 0.1 M Cr^{III} pastes, respectively. X-ray microanalysis in the TEM gave Ca:Si ratios of 1.10 ± 0.35, with a range of 0.83 to 1.49, for the blank paste and 1.15 ± 0.16, with a range of 0.95 to 1.30, for 0.1 M Cr^{III} paste.

The microstructures of the 60-day-old blank and 0.1 M Cr^{III} pastes are similar to the corresponding 1-day-old pastes, with fibrous C-S-H dominating the fracture surface (Fig. 1c,d). As in the blank pastes, the 60-day-old 0.1 M chromium-doped pastes were much less porous than the 1-day-old pastes, due to the formation of calcium hydroxide (CH) and the volume increase associated with the formation of C-S-H. Large hexagonal crystals of CH were observed in both the blank and 0.1 M Cr^{III} pastes after one day.

As the chromium concentration in the C_3S/Cr^{III} mix is increased, more distinct Cr-containing phases were observed. Fig. 2 shows an SEM micrograph and EDS spectra from a 1-M chromium nitrate sample hydrated for 1 day. In place of C-S-H, that characterized the 1-day-old blank and 0.1 M Cr^{III} pastes, rods up to 4 μm long and 0.4 μm wide highlight the microstructure (Fig. 2a). TEM studies revealed these rods to be amorphous and comprised of only Ca and Cr in highly variable ratios. The Ca:Cr mole ratio varied from 0.2 to 3.5 (Table 2). Some C-S-H regions were found to contain variable chromium concentrations (Fig. 2b). The growth of fibrous C-S-H and CH was hindered, as significantly lower amounts of these phases were detected relative to the blank and 0.1 M Cr^{III} pastes. As can be seen from Fig. 2c, the surface of the hydrated C_3S particles is devoid of fibrous C-S-H. X-ray microanalysis of Fig. 2c indicated a Ca:Si ratio of ~ 1.8.

In the 60-day-old 1 M Cr^{III} paste, the Cr-rich rods were not observed in the dense microstructures shown in Fig. 3. As evident from the EDS spectra, the paste contained large crystals of CH (region a), featureless C-S-H gel containing Cr (Fig. 3b) and C-S-H containing little or no Cr (Fig. 3c). The small Cr blips in spectra a and c were most likely derived from the surrounding Cr-containing C-S-H phase. A TEM micrograph from a 60-day-old 1 M Cr^{III} paste (Fig. 4a) revealed two types of C-S-H. The

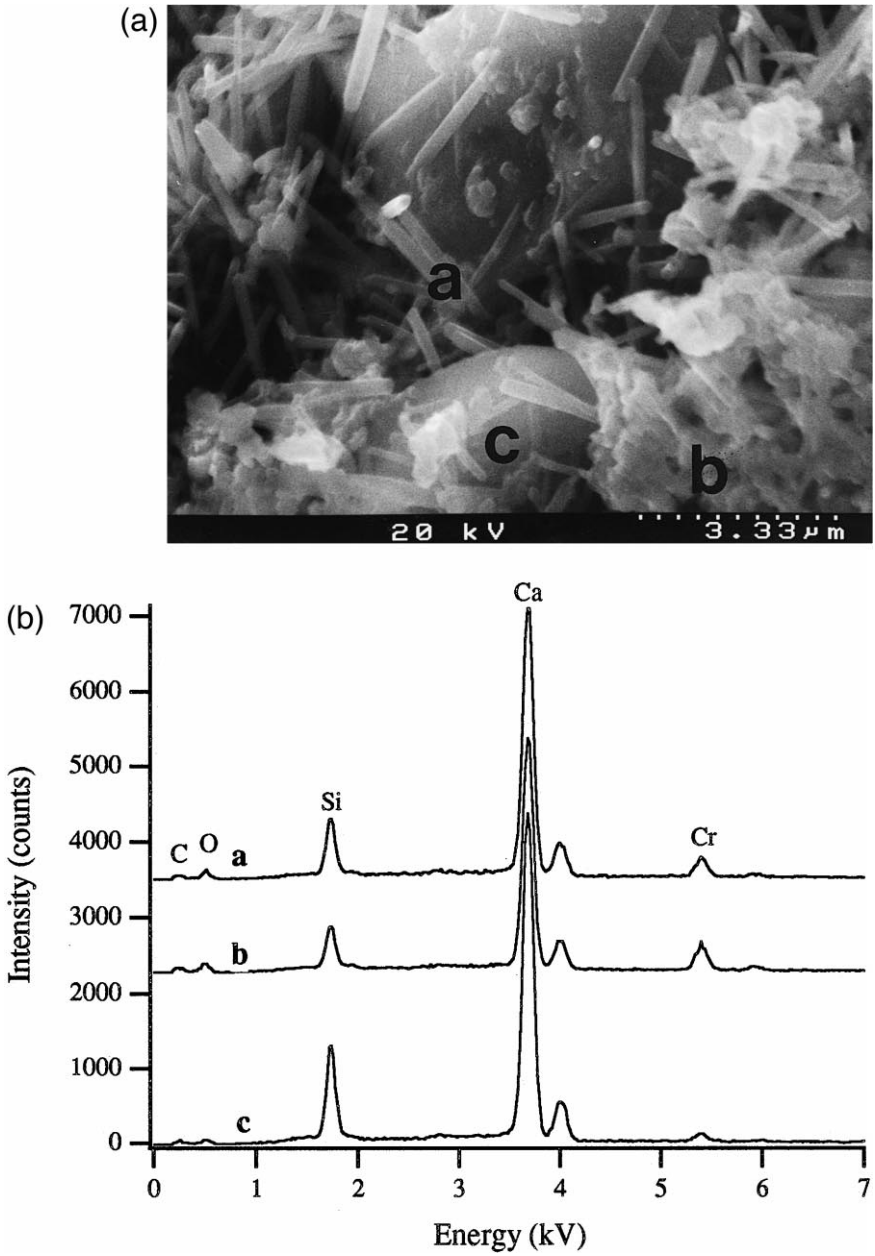

Fig. 2. SEM micrograph and EDS spectra of a fractured 1-day-old 1 M Cr^{III} paste: (a) early Ca–Cr complex rod; (b) Cr-containing C-S-H gel; and (c) C-S-H.

Table 2
Average Ca:Cr ratios in chromium-doped pastes

Sample	Ca:Cr atomic ratio $\pm \sigma$ (range)
1 M Cr^{III}: 1 day	Highly variable (0.2 to 3.5)
1 M Cr^{III}: 60 days	1.93 ± 0.11
2 M Cr^{III}: 5 min	2.92 ± 0.08
2 M Cr^{III}: 1 day	2.0 ± 0.4 (1.53–2.46)
2 M Cr^{III}: 60 days	2.2 ± 0.5 (1.47–2.79)
2.75 M Cr^{III}: 14 months (exposed)	1.95 ± 0.15 (TEM)
	1.94 ± 0.08 (SEM)

Cr-containing C-S-H I had a Ca:Si ratio ranging from 0.8 to 3.2 and high Cr concentrations. Since no crystalline CH was found in this region to account for the increase in Ca:Si ratio, some of the Ca must be associated with Cr and some Cr is possibly incorporated within the C-S-H network. The denser C-S-H II is the inner product and has a Ca:Si ratio of $\sim 1.5 \pm 0.4$, with a range of 0.8 to 2.0, and very little Cr. The apparent absence of Cr in the late inner C-S-H II suggests that most of the Cr, not forming Ca–Cr rods, is associated with C-S-H I formed during the early stages of hydration. A similar delineation between the dense inner C-S-H II and porous outer C-S-H I is depicted in the TEM micrograph of a 60-day-old blank paste in Fig. 4b. No differences were observed in the Ca:Si ratios of the two C-S-H phases.

Fig. 5a shows the relationship between the elemental concentrations, taken randomly across all detectable phases, formed in a 5-min-old 2 M Cr^{III} paste. The Ca:Si ratio in regions containing mainly C-S-H ranged from 1.12 to 2.06 with an average of 1.7 ± 0.29. This is similar to the range obtained in Cr-free regions in the blank 0.1 M and 1 M chromium samples. Localized regions containing only Ca and Cr, in other areas studied, had a Ca:Cr mole ratio of 2.92 ± 0.08. This is an indication that some type of 'Ca–Cr complex' had started forming. X-ray diffraction studies by Omotoso et al. [21] identified two types of Ca–Cr complexes. An 'early Ca–Cr complex' was detected after about 6 h and a 'late Ca–Cr complex' was observed at about 60 days of hydration. Both Ca–Cr complexes are primarily calcium chromium hydroxide nitrate hydrates. The early Ca–Cr complex was synthesized from $Ca(OH)_2$ and $Cr(NO_3)_3 \cdot 9H_2O$. The diffraction pattern of the early complex matches $Ca_6Al_2O_6(NO_3)_6 \cdot xH_2O$. This is an Aft phase that has been observed in cementitious materials. The early Ca–Cr complex was thus postulated to be $[Ca_3Cr(OH)_6(NO_3)_3]_2 \cdot (12 + x)H_2O$. The late Ca–Cr complex could not be synthesized. As can be seen from Fig. 5a, Cr concentrations are high in the analyzed C-S-H areas, indicating that most of the Cr was associated with C-S-H within the first few minutes of hydration. After 1 day, more C_3S had reacted resulting in the formation of well-defined Ca–Cr rods.

The Cr containing regions are explicitly delineated in the 60-day-old 2 M Cr^{III} paste. Fig. 5b shows two C-S-H gels containing chromium and unusually high Si concentrations. The denser C-S-H has an average Ca:Si ratio of 0.48 ± 0.09, with a narrow range between 0.39 and 0.62 (Table 1). The more porous C-S-H has a higher Ca:Si ratio, but similar variable Cr concentrations, with a Ca:Si ratio of 1.59 that ranges from 0.88 to

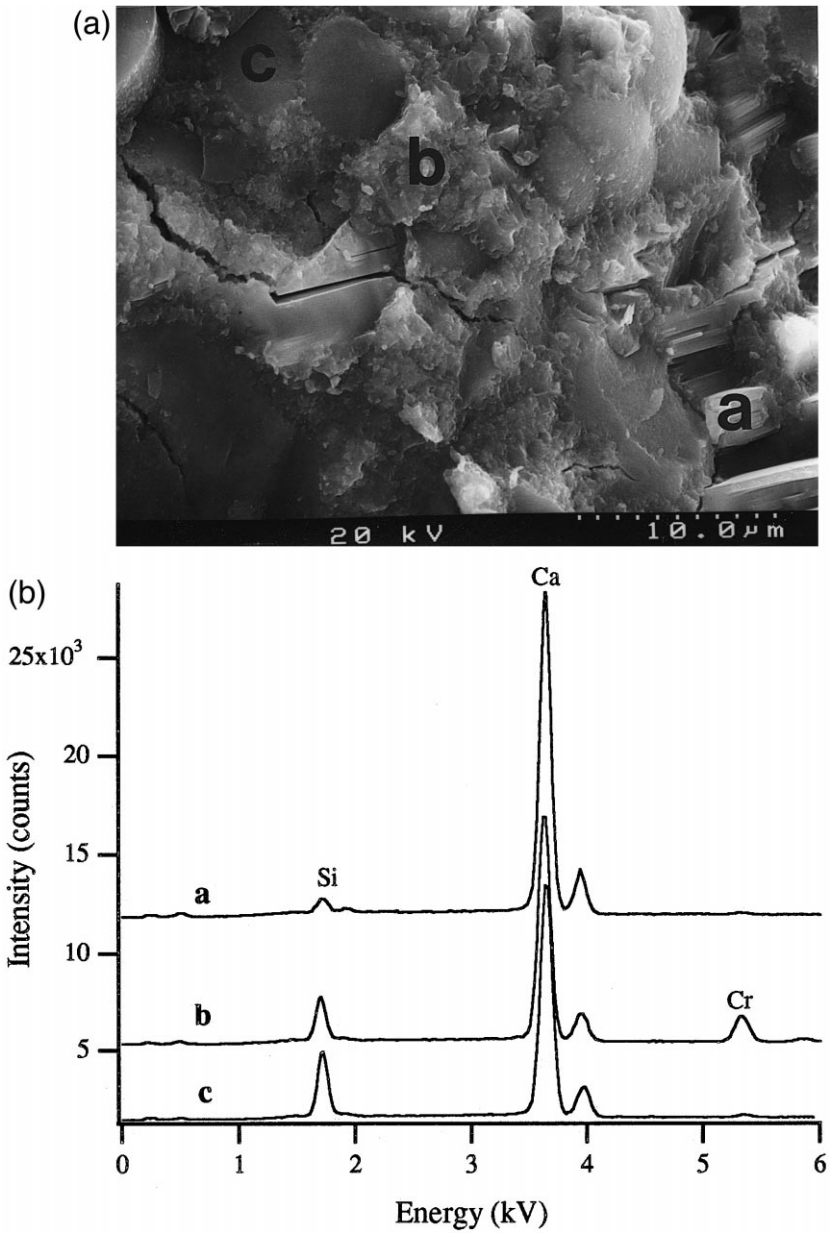

Fig. 3. SEM micrograph and EDS spectra of a fractured 60-day-old 1 M Cr^{III} paste: (a) CH; (b) Cr-rich C-S-H; and (c) C-S-H.

2.18. This is similar to the Ca:Si ratio obtained in the blank and the Cr-doped pastes discussed earlier in this section. The low Ca:Si ratio observed in the C-S-H in Fig. 5b was most probably due to the depletion of the Ca from C-S-H used for the formation of

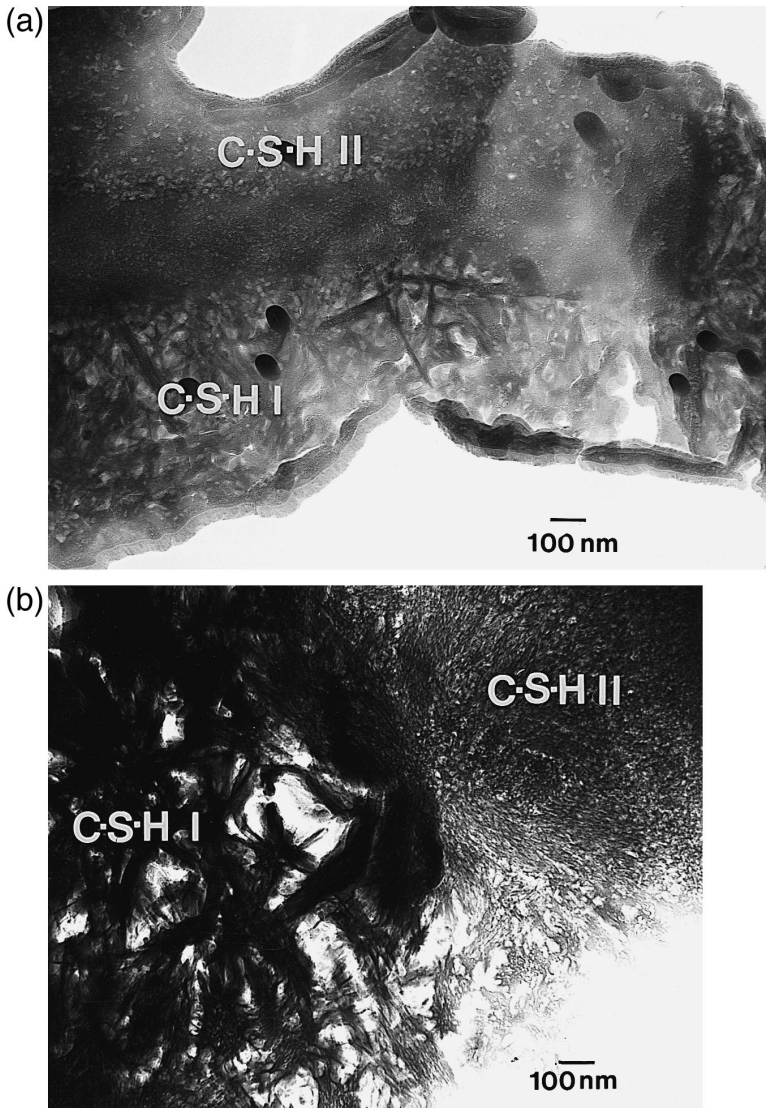

Fig. 4. TEM micrograph of 60-day-old hydrated pastes: (a) 1 M Cr^{III}; and (b) blank. C-S-H I is the fibrous C-S-H formed during the early stages of hydration and C-S-H II is a denser form of C-S-H formed during the late stages of hydration.

Ca–Cr complexes. Fig. 5c shows a TEM micrograph of the Ca–Cr rods. These amorphous rods had variable Ca:Cr ratios, varying from 1.47 to 2.79 with an average of 2.23. Considering the X-ray diffraction studies that identified both early and late Ca–Cr complexes at this stage [21], the Ca:Cr variation was not unexpected as both are located within the pores. What is unclear is that, despite the apparent crystallinity of these rods

from X-ray diffraction, selected area diffraction in the TEM shows only an amorphous ring. No Si was observed in the EDS spectra of these rods.

The microstructure of the 14-month-old 2.75 M Cr^{III} paste is similar to the 60-day-old pastes. Fig. 6a shows a TEM micrograph of a Cr-rich amorphous C-S-H gel. The average Ca:Cr ratio is 1.67, ranging between 0.82 and 2.37. The Ca:Si ratio in this area is greater than 5. Since some of the Ca is associated with Si, the actual Ca:Cr ratio would be lower than 1.67. Ca–Cr rods (late Ca–Cr complex) were also observed with a Ca:Cr mole ratio of 1.95 ± 0.15. The distribution of Cr in several phases analyzed (C-S-H with or without Cr and Ca–Cr rods) is plotted in Fig. 6b.

Fig. 7a shows a polished 14-month-old blank paste, comprising C-S-H surrounded by CH. Analysis of a corresponding polished section of 14-month-old 2.75 M Cr^{III} paste revealed some interesting microstructures. The Ca–Cr phase appeared as distinct flakes and is located in the pores surrounding C-S-H grains, as shown in an SEM micrograph (Fig. 7b). The darker flat phase is primarily C-S-H containing Cr in small but variable quantities. A line scan revealed the elemental composition of the phases. It is obvious that the C-S-H in the bottom left corner contains more Cr than the C-S-H (mid centre) surrounded by Ca–Cr flakes. The relationship between the Cr:Ca and Si:Ca atom ratios in the randomly selected regions is shown in Fig. 7c. The Ca:Si atom ratio of the mainly Cr-free clusters in the lower right region is 1.83 ± 0.15, and the Ca:Cr ratio of the Si-free Ca–Cr flakes is 1.94 ± 0.08 (upper left clusters). An interesting observation was the Ca:(Cr + Si) mole ratio, which was fairly constant, i.e. between 1.39 and 2.30 with a mode at 1.89 as shown in the histogram in Fig. 7d. With some data points between the C-S-H and Ca–Cr phases in Fig. 7c, it might appear that Cr substitutes for Si in the C-S-H gel. Another plausible interpretation is the random distribution of Ca–Cr complex in C-S-H on a microscale. The highly variable Cr concentration in the C-S-H phases observed in the TEM data, however, indicates that either possibility might be far-fetched. The evidence points more towards the localized incorporation of chromium within the C-S-H network.

The observations made through SEM and TEM X-ray microanalysis are summarized below.

(1) The early Ca–Cr complex has a Ca:Cr ratio of ~ 3 confirming it to be analogous to ettringite {Aft (Ca:(Al, Fe) ratio of 3)}, which is usually observed during OPC hydration. The late complex has a Ca:Cr atom ratio of ~ 2 suggesting a nitrate analogue of Afm type phases of OPC (Ca:(Al, Fe) ratio of 2).

(2) The Cr in the C-S-H appeared to be randomly incorporated into the C-S-H without substituting for either Ca or Si. Since the Cr-containing C-S-H appears as a single phase, chemical incorporation of Cr in the C-S-H gel is more likely than a physical mixture of C-S-H with amorphous $Cr(OH)_3 \cdot 3H_2O$ (as proposed by Kindness et al. [11]) or a calcium chromium complex on a fine scale.

3.2. FTIR spectroscopy

The complex structure of C_3S is manifest in its FTIR spectrum shown in Fig. 8a. The free orthosilicate SiO_4^{4-} has a tetrahedral (T_d) symmetry and four normal modes of vibration namely: ν_1, symmetric stretching (811–854 cm^{-1}); ν_3, asymmetric stretching

(873–997 cm^{-1}); ν_2, in plane bending (452 cm^{-1}); and ν_4, out of plane bending (513–525 cm^{-1}).

Shown in Fig. 8b–d are the infrared spectra of fully hydrated pastes (14 months old) of the blank and 2.75 M Cr^{III} (exposed and sealed). The spectra can be divided into four main groups: (i) vibrational modes due to silicate ions, (ii) vibrational modes due to water molecules and hydroxyl ions, (iii) metal–hydroxyl bending vibration and (iv) vibrational modes due to nitrate ions.

3.2.1. Silicate vibrations

In a fully hydrated blank paste, the asymmetric stretch (ν_3 (Si–O)) shifted from 939 cm^{-1} to about 981 cm^{-1}. This is expected for asymmetric Si–O–Si vibrations in dimeric and polymeric C-S-H. In the Cr-doped spectra (Fig. 8c,d), a broader band centred around 1000 cm^{-1} is observed indicating minor differences in the silicate anion environment compared to the blank paste (Fig. 8b). The weak band at 492 cm^{-1} in the blank paste can be attributed to bending modes in the polymeric silicate units. This band cannot be compared directly to the spectra of Cr^{III}-doped pastes, because it overlaps with a stronger Cr–O stretching vibration around 490 cm^{-1}. The effects of chromium on the silicate tetrahedra in hydrating C_3S may be twofold. The degree of silicate polymerization may change through competition for Ca ions by the Ca–Cr complexes and C-S-H, without the chemical incorporation of Cr ions in the C-S-H, or Cr may substitute for Si or Ca in C-S-H as postulated by some investigators [6–8]. In both cases, the silicate bands will be shifted. However, if in the second case, Si and Cr are connected through Ca polyhedra, Cr will have very little effect on silicate vibrations.

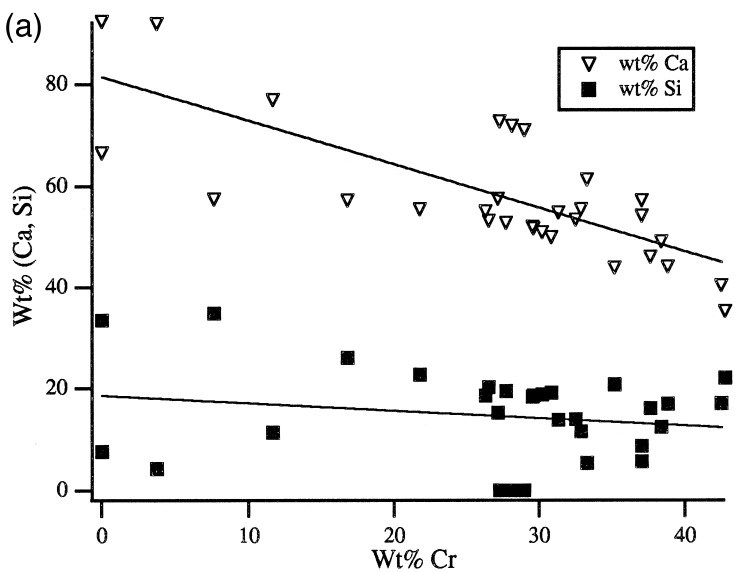

Fig. 5. (a) Variation of Ca and Si with Cr in a 5-min-old 2 M Cr^{III} paste; (b) TEM micrograph of a 60-day-old 2 M Cr^{III} paste showing Cr-containing C-S-H phases. The denser region contains very high Si concentrations; (c) TEM micrograph of a 60-day-old 2 M Cr^{III} paste showing Ca–Cr rods.

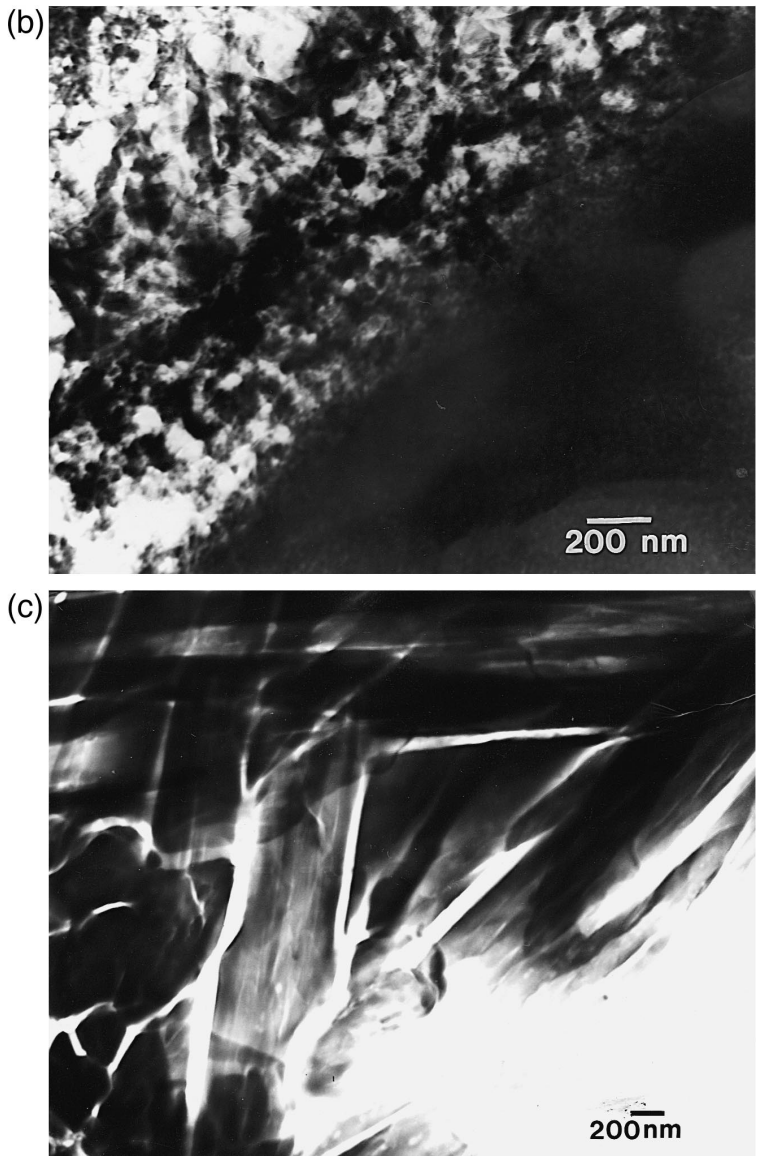

Fig. 5 (continued).

3.2.2. Water of hydration and hydroxyl ion vibrations

The fairly strong band at 1633 cm^{-1} in the spectra in Fig. 8b–d, is due to bending modes in water molecules contained in the lattice. The $\nu_1 + \nu_3$ stretching vibrations of lattice water in C-S-H are the broad band centred around 3510 cm^{-1} in the C_3S/water paste. Two broad bands at 3416 and 3548 cm^{-1} in the sealed Cr^{III} paste indicate the presence of hydration water in the early calcium chromium complex. To verify this,

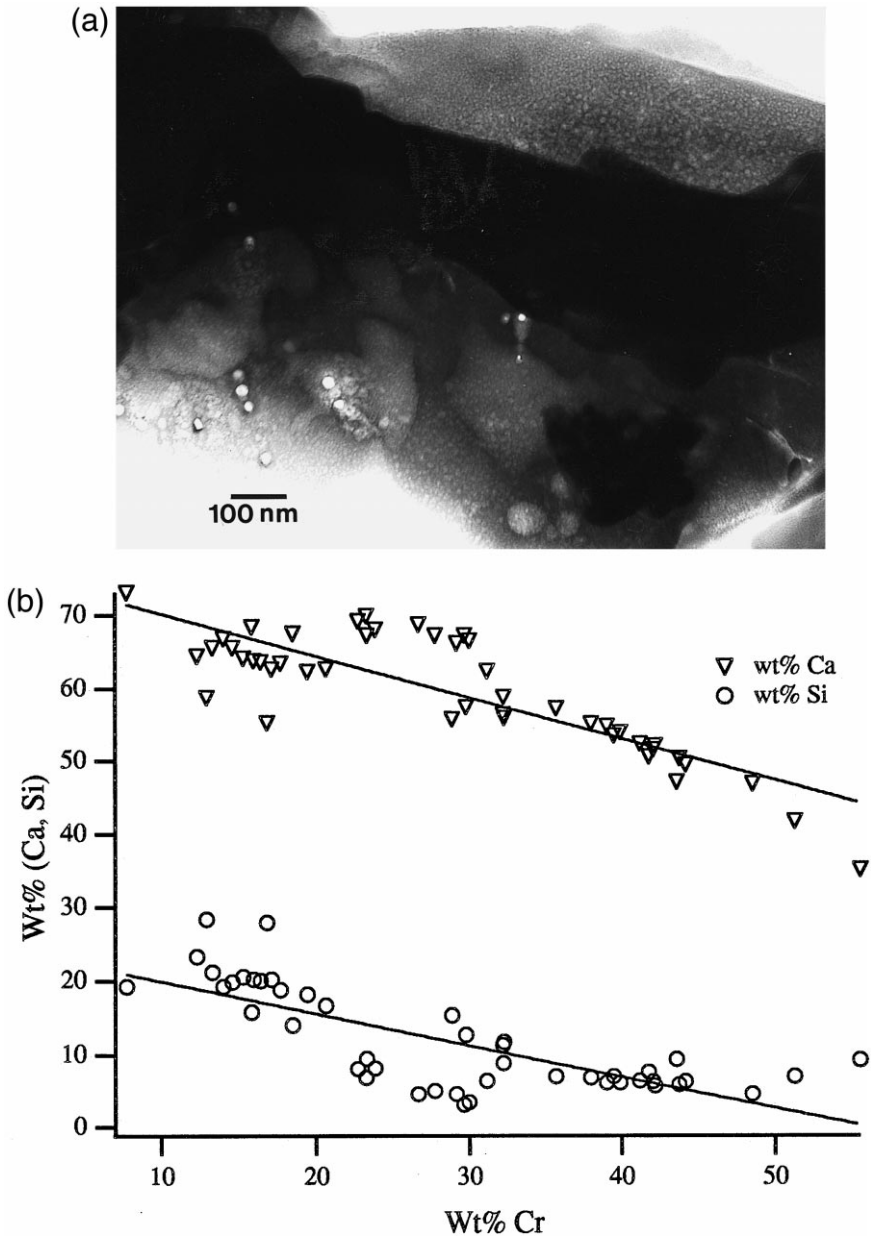

Fig. 6. (a) TEM micrograph of a 14-month-old 2.75 M Cr^{III} paste. The phase is a Cr-rich amorphous C-S-H; (b) Variation of Ca and Si levels with Cr in a 14-month-old exposed 2.75 M Cr^{III} paste. Cr containing C-S-H, Cr-free C-S-H and Ca–Cr-rich regions were analysed.

'early calcium chromium complex' was synthesized from CH and $Cr(NO_3)_3 \cdot 9H_2O$ (Ca:Cr = 3). The water vibrations in the synthesized complex (Fig. 8e) are similar to the water vibrations in the early calcium chromium complex produced in the sealed Cr^{III} paste. The exposed Cr^{III} paste has its water band centred at 3533 cm^{-1}.

The hydroxyl stretch due to CH is at 3644 cm^{-1}. This is very strong in the standard C_3S/H_2O paste (Fig. 8b) and visible in the exposed 2.75 M Cr^{III} paste (Fig. 8d) in agreement with XRD studies [15]. In hydrating C_3S paste, CH is usually noticed after about 6 h, which corresponds to the termination of the induction period [13]. The absence of CH in the sealed 2.75 M Cr^{III} paste (Fig. 8c) is suggestive of a CH formation mechanism occurring in Cr^{III} pastes different from that in normal C_3S/H_2O paste.

The very small band widths at 3588 cm^{-1} (FWHM = 10 cm^{-1}) and 3606 cm^{-1} (FWHM = 14 cm^{-1}) in the sealed 2.75 M Cr^{III} paste (Fig. 8c) indicate the presence of nonhydrogen bonded hydroxyl ions (OH^-). To further differentiate the OH bands from the broad water bands, an analogous compound to the synthesized 'early calcium chromium complex' (Fig. 8e) was prepared from deuterated water. This entailed reacting stoichiometric ratios of calcium deuteroxide $(CaOD)_2$ with $Cr(NO_3)_3 \cdot 9H_2O$ (Ca:Cr = 3) made up to 2 M with D_2O. The infrared spectrum is shown in Fig. 8f. The OD bands have shifted to 2646 and 2660 cm^{-1}, and a $\nu_H:\nu_D$ ratio of 1.36 is typical for most transition metal hydroxides [16]. Both OH and OD bands are present, since the starting $Cr(NO_3)_3 \cdot 9H_2O$ has some water. The fully hydrated exposed Cr^{III} paste (Fig. 8d) contains only one OH peak, indicating a higher site symmetry of the late calcium chromium complex than the early complex.

The nature and frequency of the vibration at 774 cm^{-1} in the Cr^{III} pastes (Fig. 8c–d) are similar to metal–hydroxyl bending modes, δ(OH), in analogous complexes such as ettringite and calcium sulphoaluminate [22]. In the deuterated complex, this peak has shifted to 538 cm^{-1} (Fig. 8f). In such case, Cr would be in octahedral coordination, i.e., $[Cr(OH)_6]^{3-}$. The bands at 530 cm^{-1} and 598 cm^{-1} in the Cr^{III} pastes (Fig. 8c,d) could not be positively assigned, but may correspond to independent sets of hydroxyls in the calcium chromium complexes.

The Cr–O stretching vibration is at 492 cm^{-1} in the sealed Cr^{III} paste and at 489 cm^{-1} in the exposed Cr^{III} paste.

3.2.3. Nitrate vibrations

The free NO_3^- ion has a planar D_{3h} symmetry. This gives rise to two NO stretching bands (ν_3 and ν_1) and two bending vibrations (ν_2 and ν_4) [23]. Of these, ν_2 and the doubly degenerate ν_3 and ν_4 are infrared active, while ν_1, ν_3 and ν_4 are Raman active. When the symmetry of the nitrate ion is lowered through complex formation, these vibrations may split, and Raman active vibrations become active in infrared. The peaks between 1320 cm^{-1} and 1450 cm^{-1} (Fig. 8c,d) belong to the asymmetric stretch (ν_3 NO_3^-). The bands split with age, according to the amount of early calcium chromium complex present in the paste (compared to the synthesized 'early Ca–Cr complex' spectrum in Fig. 8e). The splitting observed in the sealed Cr^{III} paste (Fig. 8c) indicates a lower nitrate ion site symmetry in the early calcium chromium complex and strongly bonded NO_3^-, compared to the unsplit exposed Cr^{III} paste (Fig. 8d). The presence of two doubly degenerate bands might be due to Ca and Cr coordinating NO_3^-. The band at

1047 cm^{-1} in the sealed Cr^{III} paste (Fig. 8c) is due to the symmetric NO_3^- stretching vibration, which is only active in the infrared mode when the site symmetry of the NO_3^- ion deviates from D_{3h} due to complex formation. The bending inplane vibrations are the

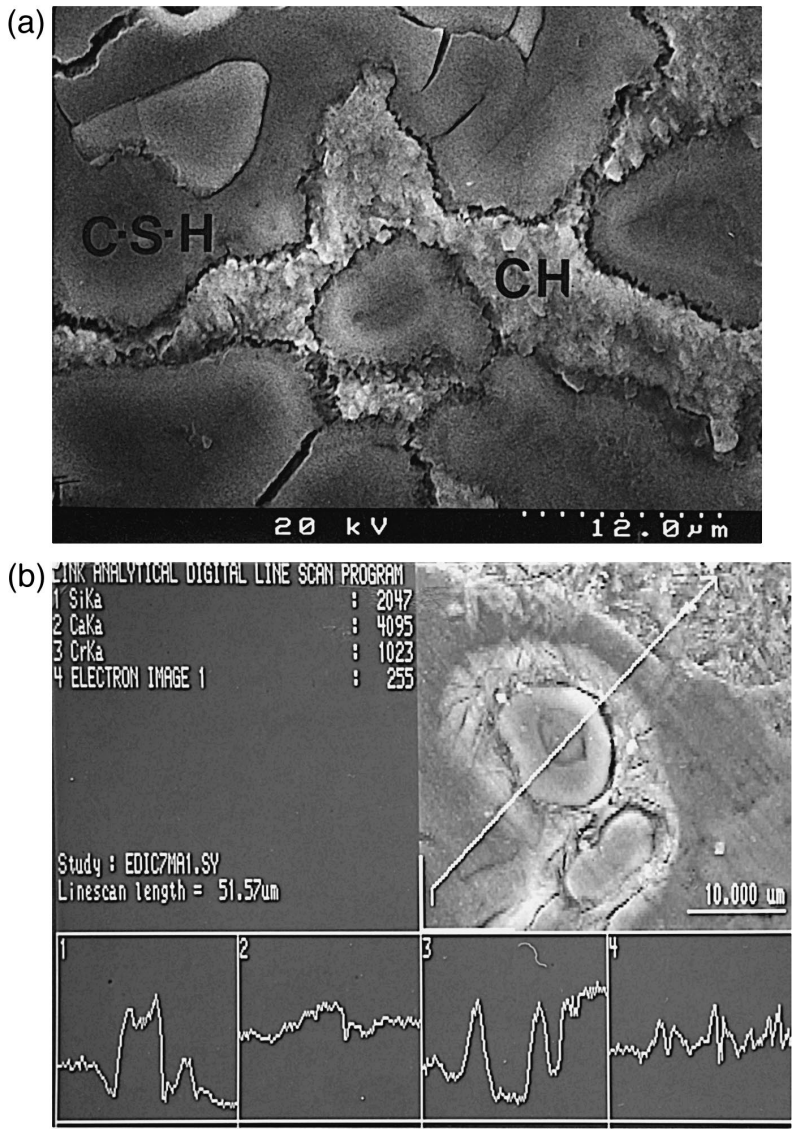

Fig. 7. (a) SEM micrograph of a polished blank paste hydrated for 14 months showing C-S-H and CH; (b) X-ray line scan of a polished 14-month-old 2.75 M Cr^{III} paste showing the relative concentrations of Ca, Cr and Si across several regions; (c) SEM/EDS analysis plot of Cr:Ca molar ratios against Si:Ca molar ratios in a typical 14-month-old 2.75 M Cr^{III} paste; and (d) frequency histogram of Ca:(Si + Cr) atomic ratios (SEM/EDS) in a 14-month-old 2.75 M Cr^{III} paste.

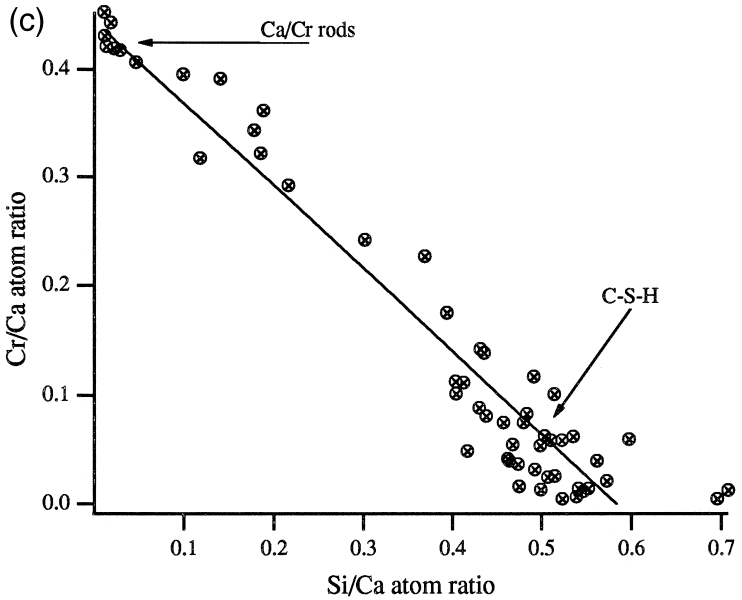

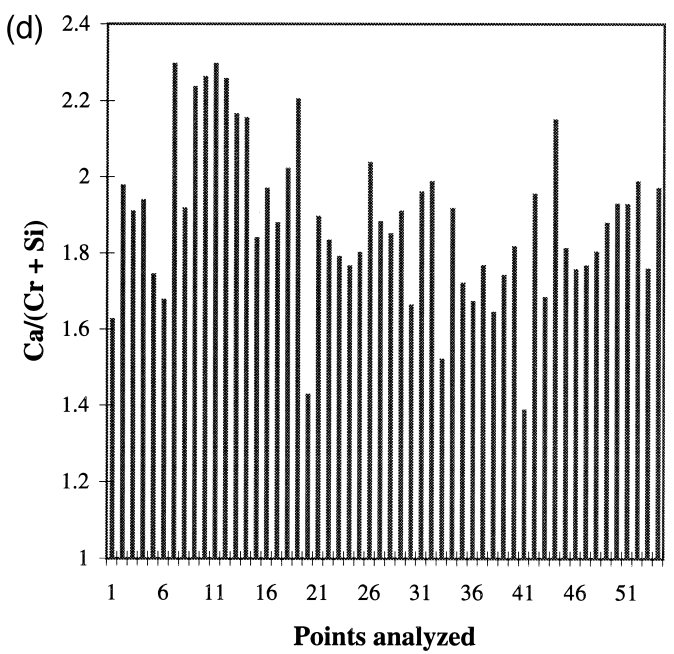

Fig. 7 (continued).

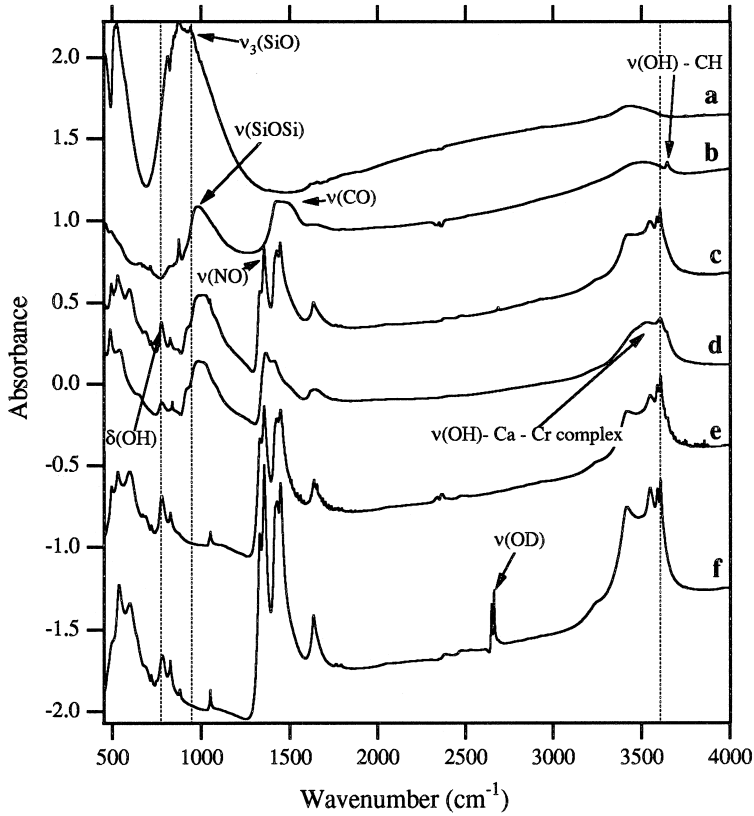

Fig. 8. FTIR spectra of fully hydrated 14-month-old pastes: (a) C_3S; (b) blank; (c) sealed 2.75 M Cr^{III}; (d) exposed 2.75 M Cr^{III} fully hydrated pastes; (e) synthesized 'early Ca–Cr complex' made from $Ca(OH)_2/Cr(NO_3)_3 \cdot 9H_2O$ in H_2O; and (f) synthesized 'early Ca–Cr complex' made from $Ca(OD)_2/Cr(NO_3)_3 \cdot 9H_2O$ in D_2O.

sharp peaks at 824 cm^{-1} (ν_2) in the sealed paste (Fig. 8c) and 834 cm^{-1} in the exposed Cr^{III} paste (Fig. 8d). Out-of-plane bending (ν_4 at 717 cm^{-1}) is only active in the sealed Cr^{III} paste. The absence of splitting in the ν_3 (NO_3^-), and the disappearance of the ν_1 (NO_3^-) vibration in the exposed Cr^{III} paste (Fig. 8d), are also indicators that the late calcium chromium complex has a higher symmetry than the early complex.

It is apparent that both complexes are primarily calcium chromium hydroxide nitrate hydrates, similar to the calcium aluminate hydroxide hydrates formed in Portland cement hydration.

The vibrational bands at 1420–1490 cm^{-1}, 870 cm^{-1} and 714 cm^{-1} in the blank paste (Fig. 8a) are due to ν_1 CO_3^{2-}, ν_2 CO_3^{2-} and ν_4 CO_3^{2-}, respectively. These arise from carbonation of CH to form calcium carbonate.

3.2.4. Rate of formation of calcium chromium complexes in 2 M Cr^{III} pastes

The infrared spectra for the exposed 2 M Cr^{III}-doped pastes hydrated for 5 min, 6 h, 1 day, 3 days and 60 days are shown in Fig. 9. The progress of hydration can be

followed by the decreasing intensities of the silicate bands and the emergence of vibrational modes of calcium chromium compounds.

The lattice water bending vibration at 1640 cm^{-1} in the spectra decreases with age. It is plausible that excess water is rejected during the formation of calcium chromium complexes from Ca^{2+}, OH^- and $[Cr(H_2O)]^{3+}$ present in the pore solution. It was observed that the samples hydrated in a humidifying chamber actually bled water even after one year. The CH band at 3644 cm^{-1} became noticeable only in the 60-day-old paste, suggesting that high concentrations of Cr inhibit the formation of CH.

In contrast to the H_2O bands that decrease with age, the intensities of the sharp OH bands at 3588 and 3606 cm^{-1} increase with age and coincide with the appearance and development of the strong δ(Cr–OH) bending vibration at 774 cm^{-1}. The intensities of the ν(OH) stretching vibrations increased continuously up to 3 days and decreased in the 60-day-old paste. These bands were completely merged in the completely hydrated exposed 2.75 M Cr^{III} paste (Fig. 8d).

The nitrate bands also change with time. Splitting of the $\nu_3(NO_3^-)$ became more evident as the concentration of the early complex increased in the system. As was the

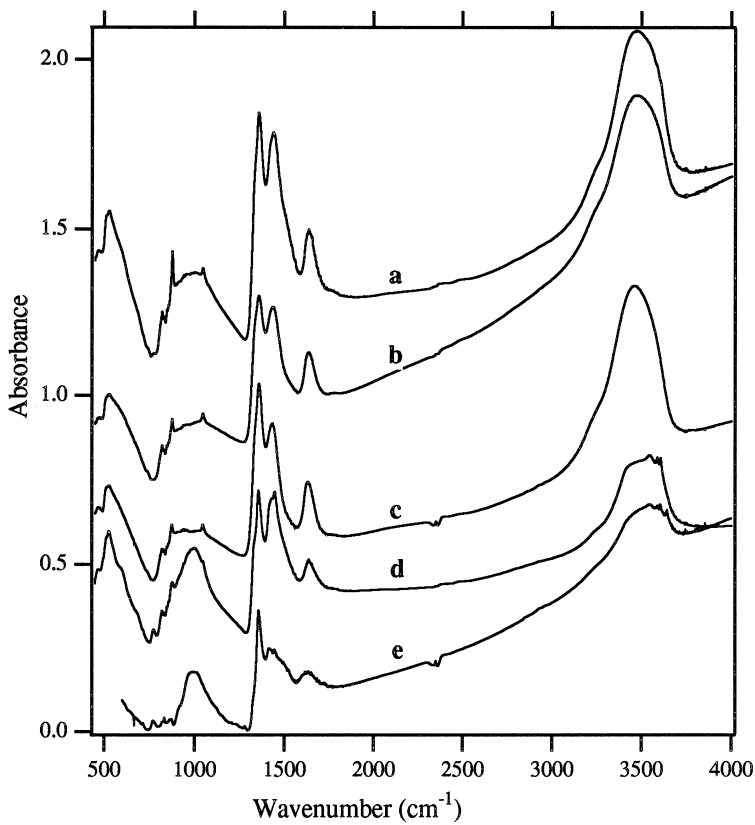

Fig. 9. FTIR spectra of exposed 2 M Cr^{III} pastes hydrated for: (a) 5 min; (b) 6 h; (c) 1 day; (d) 3 days; and (e) 60 days.

case with ν(OH) bands, less splitting was observed after 60 days, and was almost insignificant in the fully hydrated paste. Similarly, the $\nu_1(NO_3^-)$ at 1047 cm^{-1} increased in intensity up to 3 days and became smaller in the 60-day-old sample. It appeared inactive in the fully hydrated exposed Cr^{III} paste (Fig. 8d).

3.2.5. Effects of Cr^{III} concentrations on the C_3S hydration

Fig. 10 shows the spectra for 0.1 M, 1 M, 2 M and blank pastes hydrated for 1 day. Blank and 0.1 M Cr^{III} pastes possess identical silicate and lattice water vibrations. Both have quite strong CH vibrations at 3644 cm^{-1}. No CH was formed within a day in the 1 M and 2 M Cr^{III}-doped pastes. This is in agreement with the XRD results discussed in an earlier publication [21]. In the 2 M Cr^{III} paste, the asymmetric silicate stretch is much broader than in the other spectra, pointing to a greater condensation of the silicate units with increasing chromium concentrations.

The $\nu_1(NO_3^-)$ at 1047 cm^{-1}, ν_4 (NO_3^-) at 717 cm^{-1} and $\nu_1(NO_3^-)$ at 1320–1450 cm^{-1} are visible in all the Cr^{III}-doped spectra. A sharp $\nu(NO_3^-)$ band at 1384 cm^{-1}, not

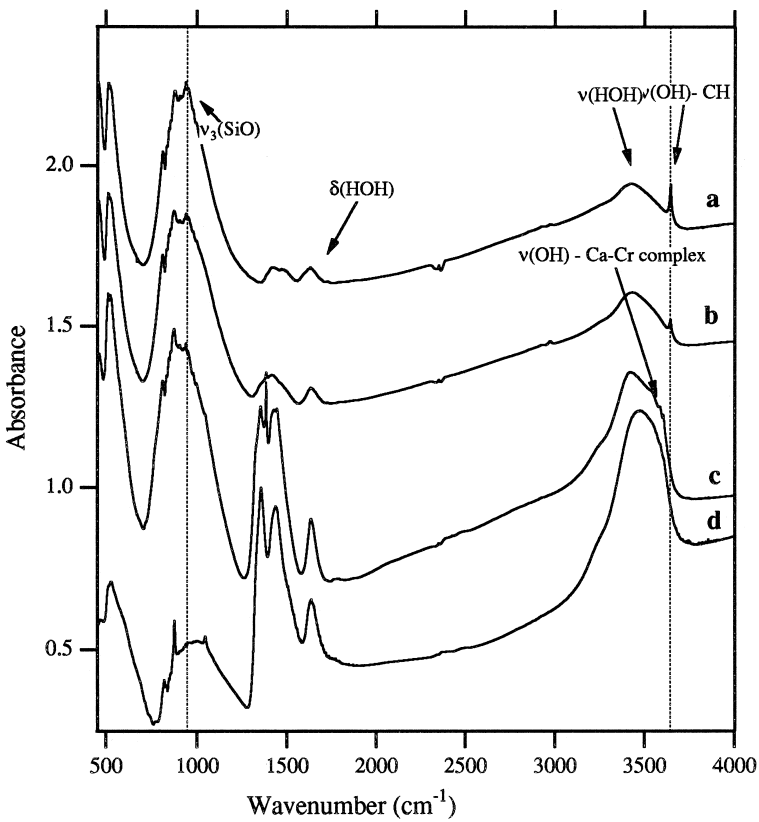

Fig. 10. FTIR spectra of varying Cr^{III} concentrations in C_3S paste hydrated for 1 day: (a) blank; (b) 0.1 M Cr^{III}; (c) 1 M Cr^{III}; and (d) 2 M Cr^{III}.

present in either of the calcium chromium complexes, was observed in both the 0.1 M and 1 M Cr^{III} pastes. The source is unclear. Both the 1 M and 2 M Cr^{III} pastes started showing splitting of the asymmetric NO_3^- stretch within 1 day. The $\nu(OH)$ stretching vibrations, characteristic of the early calcium chromium complex, are also present between 3540 and 3606 cm^{-1}. The two broad bands at 1420–1490 cm^{-1} are due to $\nu(CO_3^{2-})$ stretching vibrations of $CaCO_3$. $CaCO_3$ was produced from carbonation of CH.

Infrared spectra of 0.1 M, 1 M and 2 M Cr^{III} pastes hydrated for 60 days are shown in Fig. 11. In all the samples, most of the C_3S has reacted completely as evident in the weak intensities of the symmetric stretch (ν_1) of the orthosilicate units between 811 and 854 cm^{-1}. The bands have almost disappeared in the 1 M and 2 M Cr pastes (Fig. 11a). The intense asymmetric silicate (Si–O–Si) stretch has shifted to 955 cm^{-1} in all the spectra. A broad weak band centred at 1000 cm^{-1} is also visible in the 1 M and 2 M Cr^{III} pastes. The weak band appears as weak shoulders in the 0.1 M and C_3S/water pastes. This peak may be attributed to the polymeric silicate units in C-S-H that forms in the late stages of hydration reaction. Based on these assignments, Cr additions seem to

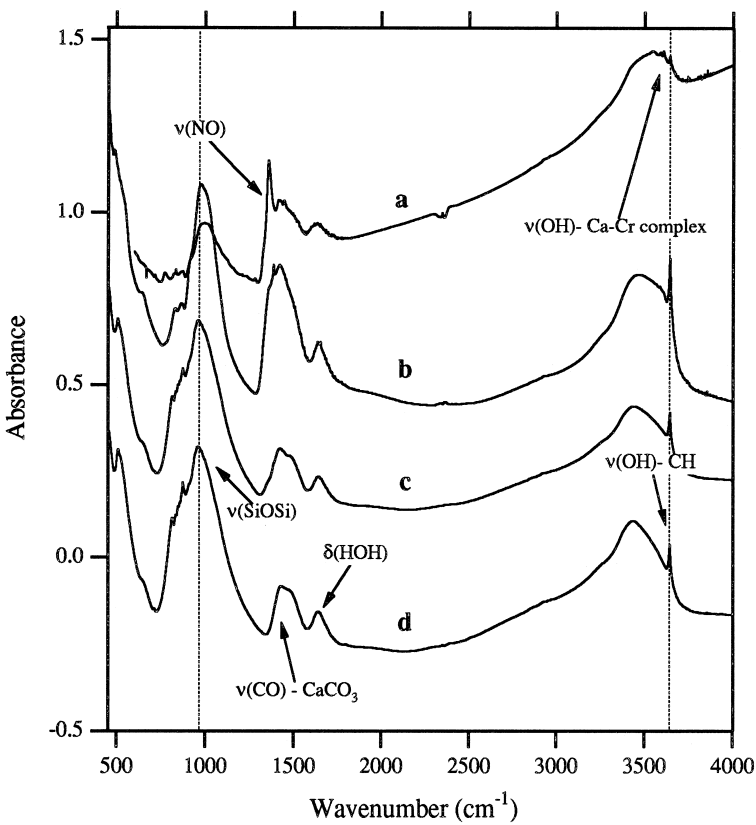

Fig. 11. FTIR spectra of 60-day-old samples: (a) 2 M Cr^{III}; (b) 1 M Cr^{III}; (c) 0.1 M Cr^{III}; and (d) blank.

promote formation of highly condensed silicate species. The strong peaks at 872 cm^{-1} and 1420–1490 cm^{-1} (Fig. 11a,b) are CO_3^{2-} vibrations in $CaCO_3$. With the exception of the 2 M Cr^{III} paste, the broad stretching vibrations of lattice water are centred around 3500 cm^{-1} in all the 60-day-old samples. The bending vibration is at 1638 cm^{-1}. The CH band at 3644 cm^{-1} is intense in all the samples, except for the 2 M Cr^{III} paste. The OH peaks due to the calcium chromium complexes are obvious in the 2 M Cr paste but barely discernible in the 1 M Cr ^{III} paste (Fig. 11b).

The following assertions can be made from the infrared absorption results of Cr^{III} pastes discussed above.

(1) Increasing chromium concentrations promotes formation of polymeric silicate units other than the dimer in C-S-H.

(2) Formation of CH is inhibited during the early stages of hydration. The inhibition increases with increasing chromium concentrations.

(3) The calcium chromium complexes are calcium chromium hydroxide nitrate hydrate complexes with $[Cr(OH)_6]^{3-}$ in octahedral positions.

(4) The late calcium chromium hydroxide nitrate hydrate has a higher symmetry and is more stable under normal hydration conditions than the early calcium chromium hydroxide nitrate hydrate.

(5) The onset of decomposition of early calcium chromium hydroxide nitrate hydrate to the formation of late calcium chromium hydroxide nitrate hydrate occurs after three days (within the time frame of experiments conducted).

3.3. Nuclear magnetic resonance spectroscopy

It was found that a very long relaxation delay (up to 24 h) was necessary to obtain good signals from the pure anhydrous C_3S. In the case of hydrated pastes containing C-S-H, however, a relaxation delay of 10 s gave satisfactory signals with a good signal-to-noise ratio. Since the silicate anion structure in C-S-H is of primary interest, a delay time of 10 s was used in all the experiments. Because the ^{29}Si nuclei in monomeric in SiO_4^{4-} in C_3S do not have sufficient time to relax, the Q_o signals between -69 and -74 ppm (representing monomeric SiO_4^{4-}) were not observed in all the spectra.

Shown in Fig. 12 are the ^{29}Si NMR spectra for Cr^{III} pastes. The end groups in silicate units (Q_1), containing dimeric silicate units (Si–O–Si linkages), gave a signal at about -79 ppm and middle units (Q_2) which contain polymeric silicate units, particularly pentamers and octamers, gave a signal at -85 ppm. These are typical of silicate units in tetrahedral coordination. The chemical shifts of octahedral silicates are usually observed to be between -200 and -250 ppm [24]. None were found in any of the samples investigated. Based on the observed chemical shifts, which are similar for the blank and Cr^{III} at all ages, it appears that very little variation exists in the silicate anion environment in the C-S-H.

There is, however, a substantial difference in the line widths of the Q_1 units in the Cr^{III} pastes compared to those in the blank pastes (Table 3). The Q_2 units have comparable width in all the spectra. During the early hydration period, saturated signals

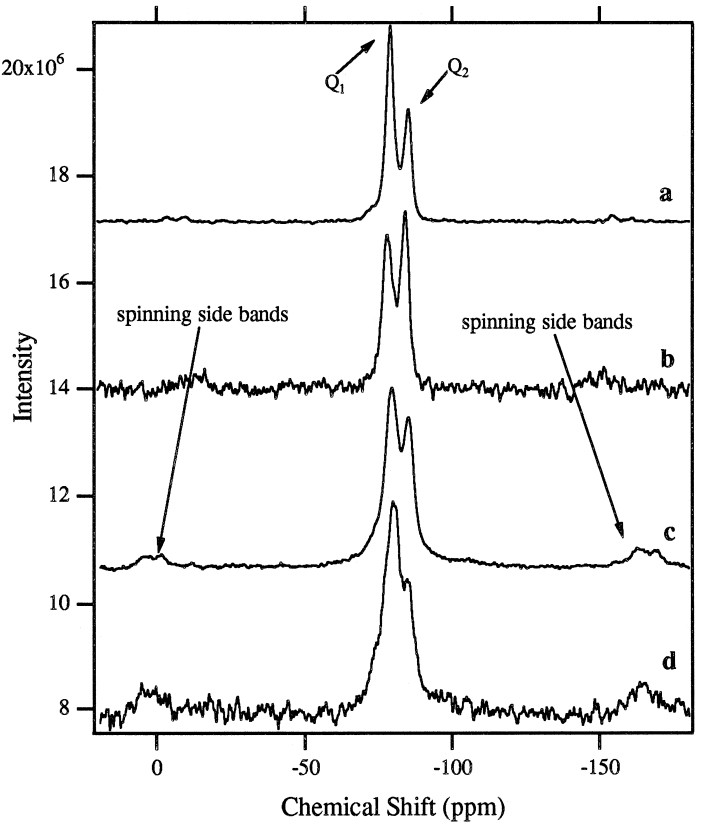

Fig. 12. ^{29}Si MAS NMR spectra of partially and fully hydrated pastes: (a) blank: 14 months; (b) 2.75 M Cr^{III}: 14 months; (c) 2 M Cr^{III}: 60 days; and (d) 2 M Cr^{III}: 3 days.

from the Q_o units may be partly responsible for the line broadening in the 3-day-old 2 M Cr^{III} paste. After 60 days, virtually all the C_3S has reacted in the 2 M Cr^{III} pastes and should therefore contribute very little to the Q_1 signal. Also, more C_3S is consumed in the Cr^{III} pastes at a given time than in the blank paste and their line widths are comparatively narrower. The paramagnetic Cr^{III} ion is thus responsible for this localized line broadening. In the Cr^{III} pastes, the Q_1 line broadening (given by the full width at

Table 3
^{29}Si chemical shift data of partially and fully hydrated chromium-doped tricalcium silicate

Sample	Q_1 (ppm)		Q_2 (ppm)		Q_2/Q_1
	Chemical shift	Line width	Chemical shift	Line width	Integrated intensity
Blank: 14 months	−78.9	3.0	−85.0	2.6	0.37
2.75 M Cr^{III}: 14 months	−78.8	3.9	−85.0	3.0	0.90
2 M Cr^{III}: 60 days	−78.9	5.6	−84.6	3.8	0.57
2 M Cr^{III}: 3 days	−79.3	6.8	−84.2	3.2	0.30

half maximum (FWHM)) is seen to decrease with age, from 6.8 ppm at 3 days to 3.9 ppm in a fully hydrated 2.75 M Cr^{III} paste. The Q_1 line width of the 14-month-old blank paste is 3.0 ppm. Variations in the Q_2 signals are less pronounced in all the spectra.

The amount of C-S-H formed increases with age (from FTIR studies), as does the concentration of Ca–Cr complexes. It is thus unlikely that Cr^{III} in the Ca–Cr complexes, even if physically mixed on a nanoscale with the C-S-H, could be responsible for this selective broadening. An obvious deduction is the unaveraged dipolar interactions between the ^{29}Si and ^{53}Cr nuclei. Because ^{53}Cr is a quadrupolar nucleus, this will not be averaged to zero by magic angle spinning (MAS). If this is the case, the line broadening should decrease with a decrease in the number of Cr nuclei in the first coordination shell of the Q_1 units. Although the broadening is less pronounced in the Q_2 units that should have a higher local Si:Cr ratio (assuming Cr is present) and the amounts of Q_1 and Q_2 increase with age, it is improbable that Cr will be located in the first or second coordination shell. Chromium located in the first or second coordination shell would mean the formation of Si–O–Cr bonds, which should give rise to distinct chemical shifts. No direct evidence of this could be seen from the spectra; however, the broad Q_1 peak could be a collection of many peaks depicting different silicate anion environments. Another indication that the broadness is induced by bonding with Cr^{III} ions is the relatively strong spinning side bands in the Cr^{III} pastes, which are symmetrical around Q_1 and Q_2. The side bands indicate greater chemical shift anisotropy and an attendant increased asymmetry in the C-S-H.

The broadening may thus be caused by a less direct mechanism than direct spin–spin interaction between the nuclei. A plausible explanation is that the ^{29}Si in Q_1 units is sensitive to further nearest neighbor interactions. These results indicate that some Cr is randomly chemically bonded in the early dimeric C-S-H. There is, however, no evidence that Cr is replacing either Si or Ca. The mere fact that tetrahedrally coordinated ($Cr^{(III)}O_4$) is rarely formed shows that replacement of tetrahedral SiO_4 by ($Cr^{(III)}O_4$) is highly improbable.

The results of trapezoidal integration of the chemical shifts are presented in Table 3. Integration was achieved by fitting a Voigt equation to the overlapping Q_1 and Q_2 peaks. This gives a better approximation of the area than a Lorenztial fit. The rate of formation of Q_1 and Q_2 follow the established trend in normal C_3S or Portland cement hydration. Q_1 forms first and later Q_2, both forming continuously throughout the hydration reaction period. The production of Q_1 and Q_2 units proceeds at a constant rate after about 30 days [25]. After about 180 days, when most of the C_3S has reacted, the Q_2:Q_1 ratio obtained by several investigators is about 0.35 [13,25]. This is similar to the Q_2:Q_1 ratio of 0.37 obtained in the fully hydrated blank paste used as a standard in these experiments. In the 2.75 M Cr^{III} fully hydrated exposed paste, the Q_2:Q_1 ratio (0.90) is higher than in the blank paste. This is more apparent when the amplitudes of Q_1 and Q_2 are compared in Fig. 12. The line broadening in the Q_1 units increases the area under Q_1. This effect is more noticeable in the 3- and 60-day-old Cr^{III}.

As previously discussed, two main hypotheses have been advanced to describe the mechanism of chromium containment in Portland cement and C_3S/alite matrices. These are summarized below.

(1) Chromium substitutes for Si or Ca (or both) in C-S-H: the stability of the C-S-H

network provides the necessary containment framework preventing chromium from leaching into solution.

(2) In the hydration of Cr^{III} doped C_3S, chromium occurs as chromium hydroxide ($Cr(OH)_3 \cdot 3H_2O$), which is insoluble in an acetic acid leaching solution.

The tetrahedral nature of the silicate anion in C-S-H makes the first mechanism suspect. The most stable configuration of Cr^{III} is in octahedral coordination, which would not be easily accommodated into tetrahedral Si sites. If Cr was to replace Ca, some Cr–O–Si bonds would form. This should give rise to distinct ^{29}Si NMR chemical shifts. Despite the high Cr concentrations used in some of our experiments, only the regular dimeric and polymeric silicate units were observed. Moreover, X-ray microanalysis should reveal high Cr/Si regions with little Ca. This was not the case in Cr-doped C_3S pastes, either polished sections or thin sections.

The wide variability and inhomogeniety of chromium contents in C-S-H regions might support the fact that insoluble $Cr(OH)_3 \cdot 3H_2O$ formed and physically mixed with C-S-H on a very fine scale. If this was the case, $Cr(OH)_3 \cdot 3H_2O$ would form within the pores during the early period of hydration. It should be very easy to isolate this phase since the pore sizes during the early period can be as large as 5 μm in diameter. Also, the hydration reaction would be slowed since $Cr(OH)_3 \cdot 3H_2O$ would form preferentially to CH. Because a certain degree of supersaturation of Ca^{2+} and OH^- is required to initiate CH formation, the reaction will be hindered until all the Cr has reacted. It has also been established that at a pH > 10.5, $Cr(OH)_3 \cdot 3H_2O$ dissolves to form anionic chromium hydroxide [26,27]. The pH of hydrating C_3S paste is ~ 12. Continued dissolution of the C_3S would result in a C-S-H of a higher than average Ca:Si ratio (~ 1.7). In fact, the reverse is the case in these experiments, where a decrease in the Ca:Si ratio was observed with increasing chromium concentrations. In addition, no crystalline $Cr(OH)_3 \cdot 3H_2O$ phase was observed in the XRD patterns and no hydroxyl absorption corresponding to $Cr(OH)_3 \cdot 3H_2O$ (amorphous or crystalline) was observed in FTIR.

3.4. Containment mechanism of Cr^{III} in C_3S pastes

The chromium nitrate solution contains $Cr(H_2O)_6^{3+}$, H^+ and NO_3^-. On contact with anhydrous C_3S, Ca^{2+}, O^{2-} and SiO_4^{4-} go into solution. The increasing amount of OH^- formed increases the pH. Because of the weak ligand field exercised by the water molecules in the hexaquo ion, rapid deprotonation of the hexaquo ion is expected to occur with OH^- and SiO_4^{4-} being potential ligand substitutes. Since no hydroxide (calcium or chromium) was found, from FTIR data, within the first few minutes of reaction, it is possible that cationic calcium and chromium ions adsorbed on the anionic silicate surface. This would cause precipitation of an unstable active calcium-chromium-silicate-hydrate. A plausible network might be for Ca polyhedra to act as a bridge for silicate tetrahedra and chromium octahedra. It has been established previously that silanol groups begin to adsorb most polyvalent metal ions (including calcium and chromium), when the pH is raised to within 1–2 points below the pH at which the metal hydroxide starts to precipitate [28–30]. As more C_3S dissolves, the pH increases, which might cause the active calcium-chromium-silicate-hydrate to dissociate into more stable states. It is believed that this initial precipitate dissociates to form stable early C-S-H and

the early Ca–Cr complex, $[Ca_3Cr(OH)_6(NO_3)_3]_2 \cdot (12 + x)H_2O$ [15]. As could be seen from the electron micrographs of 1 day old 1 M Cr^{III} doped pastes (Fig. 2), the early C-S-H forms a gel-like phase as opposed to the fibrous structure characterizing dimeric C-S-H. The early Ca–Cr complex appears as rods emanating from the gel like phase containing Ca, Si and Cr. Depending on the amount of Cr present in the paste, more $[Ca_3Cr(OH)_6(NO_3)_3]_2 \cdot (12 + x)H_2O$ forms as more Ca^{2+} becomes available in the pore solution. At the same time the C-S-H interface moves inward with Ca^{2+} and, to a lesser extent, Si^{4+} diffusing outward and H^+ diffusing inward to form the late polymeric C-S-H. The absence of Cr in the late C-S-H indicates that Cr^{3+} does not migrate across the early C-S-H interface. The reaction is accelerated possibly because of the concentration gradient developed between the reactive C_3S grain and the pore space harboring a reactive calcium-chromium-silicate phase. The high Ca content of the Ca–Cr complex necessitates a reduction in the amount of Ca^{2+} available to form C-S-H, that has an average Ca:Si ratio ~ 1.7. This will result in the increased formation of highly condensed C-S-H, which is consistent with ^{29}Si NMR studies showing that more Q_2 (polymeric C-S-H) than Q_1 (dimeric C-S-H) forms in a fully hydrated paste. X-ray microanalysis in the TEM also indicates the absence of Cr in the late C-S-H and a wide variability of Ca:Si ratios in Cr-free C-S-H. Many areas with Ca:Si ratios < 0.5 were observed. This is much lower than the lower limit of ~ 0.8 obtained in the blank pastes. The ^{29}Si NMR chemical shift data also indicate line broadening of the Q_1 units, which reduces with age. This is a further indication that most of the Cr is chemically incorporated in the C-S-H at a molecular level during the early stages and gradually precipitates out with age.

If the reaction is carried out in an enclosed environment with no secondary source of moisture, as soon as most of the Cr is complexed, the normal hydration reaction continues with the formation of CH and C-S-H. The final product will thus contain $[Ca_3Cr(OH)_6(NO_3)_3]_2 \cdot (12 + x)H_2O$, CH, C-S-H (Cr-free) and some stable C-S-H containing highly localized Cr. The Cr containing C-S-H forms during the early stages of hydration. On the other hand, if the paste is exposed to a humid atmosphere, the highly reactive components will absorb moisture. This causes $[Ca_3Cr(OH)_6(NO_3)_3]_2 \cdot (12 + x)H_2O$ to decompose to give the late Ca–Cr complex (Ca:Cr ratio = 2) and CH. The CH formed from this reaction is visible as crystals growing from the supersaturated solution that collects on the paste. Total decomposition of the early Ca–Cr complex will occur over time. In both cases, the residual chromium associated with C-S-H should be unaffected.

The formation of the Ca–Cr complexes depends on the concentration of chromium in the hydrating paste. Thus, at the lower chromium concentrations of ~ 0.1 M Cr^{III}, typical of chromium waste streams, small amounts of the Ca–Cr complexes are formed, which may not be visible within the detection limits of XRD and FTIR spectroscopy. Some of the Cr will also be chemically incorporated in the C-S-H as discussed above.

4. Conclusions

(1) Small amounts of Cr^{III} are inhomogeneously chemically incorporated in the early C-S-H, independent of the hydration environment and, to a lesser extent, the concentra-

tion of Cr in the reacting mixture. The Cr^{III} octahedra are possibly connected to the silicate tetrahedra through Ca–O linkages.

(2) Two forms of Ca–Cr complexes are confirmed to be forming. A nitrate analogue of an Aft-type phase $[Ca_3Cr(OH)_6(NO_3)_3]_2 \cdot (12 + x)H_2O$ (early Ca–Cr complex) forms during the early stages of hydration. Another complex, termed 'late Ca–Cr complex' formed in the later stages of hydration. This is presumably an analogue of Afm-type cement phases.

(3) Results of NMR and FTIR studies indicate that increasing Cr concentration increases the condensation of the silicate units. This is manifested in the increased ratio of polymeric C-S-H to dimeric C-S-H. The rate of C_3S reaction is also increased with increasing Cr additions.

(4) NMR and TEM data indicate no evidence of Cr^{III} replacing Si in tetrahedral sites.

(5) $Cr(OH)_3 \cdot 3H_2O$ (crystalline or amorphous) was not observed at any stage of hydration reaction.

Acknowledgements

The authors wish to thank the Department of Natural Resources Canada (CANMET), and the Natural Sciences and Engineering Research Council of Canada (NSERC) for providing the financial support for this project.

References

[1] R.B. Williamson, Prog. Mater. Sci. 15 (1972) 89.
[2] S. Diamond, Hydraulic cement pastes: Their structure and properties, Conference Proceedings of the Cement and Concrete Association, 1976, p. 2.
[3] S. Goto, M. Daimon, G. Hosaka, R. Kondo, J. Am. Ceram. Soc. 59 (1976) 281.
[4] B. Marchese, Cem. Concr. Res. 7 (1977) 9.
[5] B. Marchese, J. Am. Ceram. Soc. 61 (1988) 349.
[6] R.B. Heimann, D. Conrad, L.Z. Florence, M. Neuwirth, D.G. Ivey, R.J. Mikula, W.W. Lam, J. Hazard. Mater. 31 (1991) 39.
[7] D.G. Ivey, R.J. Mikula, W.W. Lam, M. Neuwirth, D.J. Conrad, R.B. Heimann, in: R.D. Spence (Ed.), Proceedings of the Chemistry and Microstructure of Solidified Waste Forms, Lewis Publishers, Boca Raton, FL, 1993, p. 123.
[8] M.Y.A. Mollah, Y.-N. Tsai, T.R. Hess, D.L. Cocke, J. Hazard. Mater. 30 (1992) 273.
[9] C. Tashiro, H. Takahashi, M. Kanaya, I. Hirokid, I. Yoshida, Cem. Concr. Res. 7 (1977) 288.
[10] L.G. Butler, F.K. Cartledge, H.C. Eaton, M.E. Tittlebaum, in: R.D. Spence (Ed.), Proceedings of the Chemistry and Microstructure of Solidified Waste Forms, Lewis Publishers, Boca Raton, FL, 1993, p. 151.
[11] A. Kindness, A. Macias, F.P. Glasser, Waste Manage. 14 (1994) 3.
[12] I.G. Richardson, G.W. Groves, Cem. Concr. Res. 23 (1993) 131.
[13] H.F.W. Taylor, Cement Chemistry, Academic Press, London, 1990.
[14] D.L. Rayment, E.E. Lachowski, Cem. Concr. Res. 14 (1984) 43.
[15] O.E. Omotoso, Doctoral thesis, University of Alberta, Edmonton, 1996.
[16] Y.I. Ryskin, in: V.C. Farmer (Ed.), The Infrared Spectra of Minerals, Mineralogical Society, London, 1974, p. 137.
[17] E. Lippmaa, M. Magi, A. Samson, G. Engelharrdt, A.R. Grimmer, J. Am. Chem. Soc. 102 (1980) 4889.

[18] E. Lippmaa, M. Magi, M. Tarmak, W. Wieker, A.R. Grimmer, Cem. Concr. Res. 12 (1982) 597.
[19] I. Jawed, J. Skanly, J.F. Young, in: P. Barnes (Ed.), Structure and Performance of Cement, Applied Science Publ., Barking, 1983, p. 237.
[20] N.L. Thomas, J. Mater. Sci. 22 (1987) 3328.
[21] O.E. Omotoso, D.G. Ivey, R.J. Mikula, Cem. Concr. Res. 26 (1996) 1369.
[22] J. Bensted, S.P. Varma, Cem. Technol. 4 (1973) 112.
[23] K. Nakamoto, Infrared and Raman Spectra of Inorganic and Coordination Compounds, 4th edn., Wiley, New York, 1986.
[24] A.R. Grimmer, F. Von Lampe, Chem. Phys. Lett. 132 (1986) 549.
[25] N.J. Clayden, C.M. Dobson, G.W. Groves, C.J. Hayes, S.A. Rodger, Br. Ceram. Soc. Proc. 35 (1984) 55.
[26] R. Giovanoli, W. Stadelmann, Thermochim. Acta 7 (1973) 41.
[27] L. Spiccia, W. Marty, Inorg. Chem. 25 (1986) 266.
[28] R.O. James, T.W. Healy, J. Colloid Interface Sci. 40 (1972) 65.
[29] L.L. Olsen, C.R. O'melia, J. Inorg. Nucl. Chem. 35 (1973) 1977.
[30] P.W. Schindler, B. Furst, R. Dick, P.U. Wolf, J. Colloid Interface Sci. 55 (1976) 469.